Numerical analysis of subcritical evaporation and transcritical mixing of droplet using a tabulated multicomponent vapor-liquid equilibrium model

Ping Yi[1,2], Sajad Jafari[1,2], Songzhi Yang[1,2], Chaouki Habchi*[1,2]
[1]IFP Energies nouvelles, 1 et 4 avenue de Bois-Préau, 92852 Rueil-Malmaison, France
[2]Institut Carnot IFPEN Transports Energies, 1 et 4 avenue de Bois-Préau, 92852 Rueil-Malmaison, France
*Corresponding author: Chaouki.Habchi@ifpen.fr

Abstract
In this paper, a fully compressible real-fluid and homogeneous equilibrium model (HEM) has been developed, in which the two-phase characteristics are obtained using a tabulated multicomponent vapor-liquid equilibrium approach. This classical HEM model consists of four balance equations posed in terms of mass density, partial species density, momentum, and internal energy (e). The thermodynamic properties of the mixture are calculated as a function of temperature, pressure and species composition (z_i) based on the Peng-Robinson equation of state. Most importantly, a bijective look-up table linking (ρ, e) and (T, P) is constructed using a computationally efficient isothermal isobaric (TPn) flash. This look-up table also includes various thermodynamic derivatives such as sound speed, heat capacity as well as the transport properties. During the simulation, all thermal and transport properties are linearly interpolated using (T, P, z_i). This tabulation approach has been successfully applied to the investigation of subcritical evaporation and transcritical mixing characteristics of spherical n-dodecane droplets in a nitrogen ambient. Primarily, an isolated droplet with uniform initial temperature is put into a moderate ambient condition ($P_{amb.} = 62$ bar, $T_{amb.} = 700$ K), in which it undergoes a classical evaporation process with the continuous diameter reduction. Then, the droplet is injected into a high temperature and pressure condition ($P_{amb.} = 102$ bar, $T_{amb.} = 1200$ K), in which the droplet firstly remains spherical for a while, and then deforms to an olive shape. The predicted results are shown to be in good agreement with the recent experimental findings. The thermodynamic analysis also demonstrates that the droplet has entered the two-phase regime with a diffused interface in which vapor and liquid coexist. This proves that the experimentally observed clouds around the droplet at ($P_{amb.} = 102$ bar, $T_{amb.} = 1200$ K) is still mainly generated by evaporation, and not due to diffusive mixing, even though the initial ambient gas is significantly above the n-dodecane critical point ($P_c = 18.1$ bar). The transition from the subcritical classical evaporation to the supercritical mixing regimes is also discussed in this work based on thermodynamic arguments.

Keywords
Homogeneous equilibrium model, Thermodynamic tabulation, Subcritical evaporation, Transcritical transition, supercritical mixing

1. Introduction

Liquid fuel injection is a common process that exists in many energy conservation devices, such as in the diesel and gas turbine engines. Some practical engines operate at supercritical conditions. However, the injected fuel may be at subcritical, transcritical or supercritical state during the injection, mixing and evaporation processes. In these engines, shadow areas still exist in such a way that the injected fuel temperature is well below its critical temperature while both in-cylinder pressure and temperature exceed the fuel's critical points. Most studies in the literature termed this phenomenon as transcritical injection. The issue of thermodynamic non-idealities near the critical point is one of the main challenges to model these phenomena [1,2]. However, this raises a question about whether the multicomponent mixture really transits to the supercritical state relative to the mixture critical point in the engine operating conditions? Up to now, this issue has not been resolved yet[3,4]. Moreover, there are also some concerns about the superheated liquid which may induce bubble nucleation, cavitation and violent phase change inside the liquid. These phenomena may further produce serious consequences such as explosion, fires or toxic exposure which will hence bring in immense damages [5].

Generally, the transition criterion from the evaporating subcritical to the diffusive mixing regime is not rigorously following the variation of the pure fuel critical point. Several studies have provided important insights on the transcritical behaviors, as well as the limitations of current theoretical modelling and numerical simulations of such flows [6,7]. The available experimental studies have stimulated great interest in exploring the multicomponent real fluid transition process. Crua et al. [7] proposed a transition criterion of $T_r\sqrt{P_r}$ based on the experimental phenomena (Figure 1). Yang et al. [4] pointed out that the flow transport process under supercritical conditions

exhibits distinct behaviours compared to those under subcritical conditions. Bellan [2] presented a comprehensive review of droplet dynamics, thermodynamics, and transport properties at supercritical conditions. Under the supercritical case, the droplet sphericity diminishes sharply, and the temperature increases continuously during the diffusive mixing process. However, most supercritical studies are discussed with respect to the fuel critical point (Figure 1) [10-12]. The real physics involved in the transition from subcritical to the mixture thermodynamic supercritical condition has not been well addressed. The lack of fundamental understanding of the real transcritical spray is due to the considerable challenges involved in developing appropriate experiments and relevant multiphase flow models.

Researchers have attempted to develop various two-phase flow models, with the numbers of transport equations ranging from three to seven depending on the initial equilibrium assumptions [13-17]. Among of them, the four-equation models due to their high efficiency are very prevalent for cavitation and spray simulations [18]. The four-equation model is composed of three conservation laws for mixture quantities (mass, momentum, energy) in addition to eventual partial density transport for multicomponent problems. These equations are usually solved along with a phase change source term, as in the Homogeneous Relaxation model [35], for instance. The main issue in such models is to accurately estimate the phase change term for the classical subcritical evaporation, and it is unable to transit to supercritical single-phase mixing regime. Yang et al. [4] and Yi et al. [20] have recently employed a specific real-fluid multicomponent vapor-liquid equilibrium solver, which includes a stability test to distinguish the single-phase and two-phase flows; and implements isothermal-isobaric and isoenergetic-isochoric flash to predict the phase change source term, along with the two-phase equilibrium temperature, pressure and phase compositions. However, in practice, it is proved that the complexity of the cubic EOS and solving flash problems for all grid cells over all nonlinear iterations and time steps are very computational demanding [20,21,22]. Therefore, a more robust and efficient tabulation approach needs to be developed to elevate the computational efficiency of the thermodynamic solver.

In the literature, there are many studies focused on the thermodynamic property tables rather than the multicomponent vapor-liquid equilibrium tabulations. Azimian et al. developed an artificial neural network for generating steam tables [23]. Wang et al. [24, 25] proposed a spline-based tabulation method for water and steam. Khatami et al. [26] introduced a two-dimensional phase-oriented interpolation approach to deal with the discontinuous values at the phase boundary, which can improve the accuracy compared to the previous methods. Brown et al. [27] also suggested an adaptively inverse interpolation approach.

The present study describes a robust as well as efficient bijective tabulation method as a simple look-up procedure for accurate interpolations over the entire range of fluid thermodynamic states. It involves the single-liquid like, single-gas like, as well as two-phase states. This bijective tabulation is implemented into a four-equation HEM model. A three-dimensional isothermal-isobaric TPn-table is chosen mainly to replace the costly iterative methods of the TPn flash. The second reason but not least is to be able to simulate for different fuels and surrogates by using an existing flash library instead of the hard coding a TPn flash for each of them.

In order to validate the newly developed methodology, this work attempts to conduct a comprehensive investigation about the evaporation behaviours of a n-dodecane droplet injected into a supercritical nitrogen ambient over a broad range of temperature and pressure conditions. This paper is organized as follows. Section 2 describes the numerical and theoretical methods including the tabulation and thermodynamic ingredients. Then, the subcritical and transcritical evaporation are discussed and qualitatively compared with the experimental images from Crua et al [7] in Section 3. Finally, the conclusions are presented.

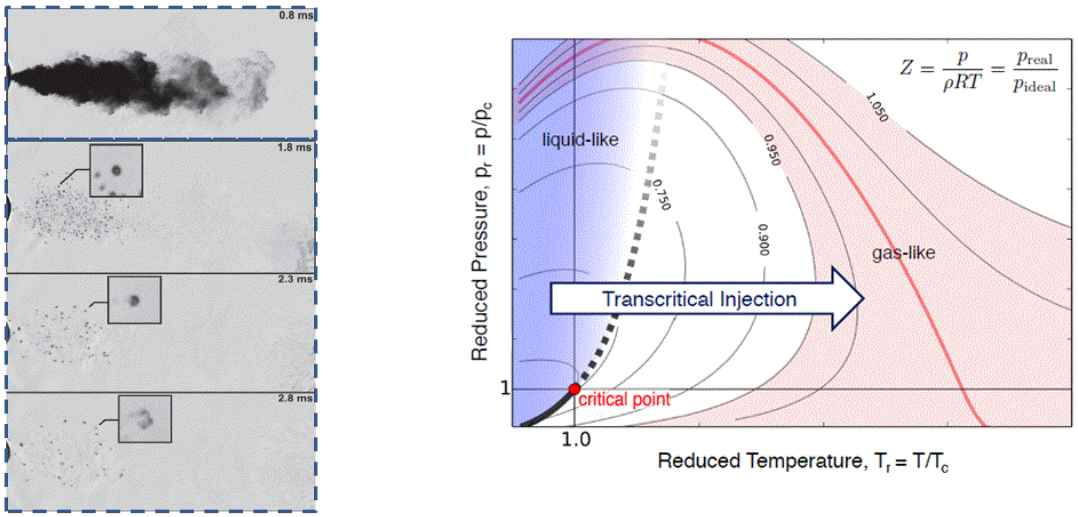

Figure 1. Transcritical injection: (Left) experimental images from [7]. (Right) typical single-phase P-T diagram [28].

2. Numerical model

2.1 Homogenous equilibrium model

In this study, we solve the three-dimensional fully compressible Navier–Stokes equations, which are based on the thermal and mechanical equilibrium. The governing equations are as following.

$$\frac{\partial \rho}{\partial t} + \frac{\partial \rho u_i}{\partial x_i} = 0 \tag{1}$$

$$\frac{\partial \rho Y_m}{\partial t} + \frac{\partial \rho Y_m u_j}{\partial x_j} = \frac{\partial}{\partial x_j}\left(\rho D \sum_m \frac{\partial Y_m}{\partial x_j}\right) \tag{2}$$

$$\frac{\partial \rho u_i}{\partial t} + \frac{\partial \rho u_i u_j}{\partial x_j} = -\frac{\partial P}{\partial x_i} + \frac{\partial \sigma_{ij}}{\partial x_j} \tag{3}$$

$$\frac{\partial \rho e}{\partial t} + \frac{\partial \rho e u_j}{\partial x_j} = -P\frac{\partial u_j}{\partial x_j} + \sigma_{ij}\frac{\partial u_i}{\partial x_j} + \frac{\partial}{\partial x_j}\left(K\frac{\partial T}{\partial x_j}\right) + \frac{\partial}{\partial x_j}\left(\rho D \sum_m h_m \frac{\partial Y_m}{\partial x_j}\right) \tag{4}$$

where ρ, u, P, T, e are mixture density, velocity, pressure, temperature and specific internal energy, respectively; Y_m and h_m are the mass fraction and enthalpy of each species m, respectively. The above system is closed by a composite Peng-Robinson equation of state PR-EoS, as explained in [20] using tabulated thermal and transport properties. The thermal properties are estimated based on PR-EoS and the ideal reference data are provided by NIST. The laminar transport properties, thermal conductivity, K and viscosity are calculated using Chung et al. correlations [28]. Then, the laminar diffusion coefficient is estimated using a given Schmidt number as **D=*ν*/Sc**. The details are introduced as follows.

2.2 Tabulation approach

Because of the complexity of real fluid behaviour modelled with non-linear equation of State (EoS), such as PR-EoS, and the underlying computational demanding isoenergetic-isochoric flash (UVn) algorithm in the multi-phase flow simulations [21, 22], a more simplified and efficient tabulated phase equilibrium method is proposed in this work. It is based a bijective look-up table linking (ρ, e) and (T, P) generated using a robust isothermal isobaric (TPn) flash [4, 20]. In the tabulation, the mixture density (ρ) and specific internal energy (e) are computed as $\rho = \sum \alpha_p \rho_p$ and $e = \sum \alpha_p \rho_p e_p / \rho$, respectively; where α_p denotes the volume fraction of phase p ($p = 1$ is liquid phase, $p = 2$ is gas phase). The simplistic inverse-distance weighting (IDW) [29] method is used for three-dimensional (3D) tabulation. This method is based on the assumption that the attribute value of unsampled point is the average weight of known values in the neighbourhood, and the weight is inversely related to the distances (d) between the prediction location and sampled locations. As a first step, only the two-component mixtures are considered and the 3D-Tabulation inputs are temperature, pressure, and mass fraction (T, P, Y). Taking one-dimension (i) as an example, the unknown values $F(S_i^*)$ at the locations S_i^* are interpolated linearly based on the values of sampled locations (S_i), as follows,

$$F(S_i^*) = \sum_{i=1}^{2} \lambda_i F(S_i) \quad , \quad \lambda_i = d_i / \sum_{i=1}^{2} d_i \quad , \quad F(S_{i,j,k}^*) = \sum_{k=1}^{2} \lambda_k \left[\sum_{j=1}^{2} \lambda_j F(S_i^*)\right] \tag{5}$$

2.3 Real-fluid multicomponent VLE tabulation

In this work, the multicomponent vapor-liquid equilibrium (VLE) table is generated using a thermodynamic solver developed by Yang et al. [4] in the in-house code, IFP-C3D [30]. The algorithms summarized below follow two steps: (A) The phase state at each group of temperature, pressure and feed is determined based on the phase stability analysis or Tangent Plane Distance (TPD) [31]; (B) A robust isothermal-isobaric (TPn) flash [22] coupled with PR EoS is performed to compute the thermodynamic equilibrium internal energy, density and composition of each phase, as well as the necessary derivatives, such as the sound speed, and the transport properties.

3. Description of the droplet evaporation and mixing test case

Although many studies have been conducted to examine the droplet evaporation behaviors under static and convective conditions [5,32-34], effects of ambient conditions on the droplet dynamics have not yet been well reported especially for the extreme conditions higher than the fuel critical point. Therefore, the current HEM model considering the multidimensional flow motions is applied to gain a thorough examination of underlying droplet behaviors during its lifetime. This droplet lifetime includes the dynamic deformation, evaporation, and transition from subcritical to supercritical with respect to the critical point of mixture. For simplicity, only nitrogen is considered in the initial ambient to avoid reaction. The droplet is composed of almost pure n-dodecane, the mass fraction is 0.999999, the initial temperature is 363 K. The detailed information is listed as in Table 1. In Case 1,

the droplet is assumed stagnant in a relatively low temperature condition of 700 K, the ambient pressure is 62 bar. The droplet diameter in Case 1 is around 38 µm [7]. In Cases 2 and 3, the ambient temperature and pressure are much higher than the critical points of n-dodecane. The initial droplet diameter and velocity in the experimental observations are around 60 $\boldsymbol{\mu m}$ and 0.2 m/s. In order to investigate the effects of velocity on the moving droplet performance, one case with high velocity of 2 m/s is simulated. The simulation is carried out in box (0.3 × 0.3 × 0.3 mm) in Case 1 and a periodic canal (0.5 × 0.32 × 0.32 mm) in Case 2 to 4, with a uniform mesh size equal to 3 µm. DNS simulations are therefore performed (without turbulence subgrid scale model) because of the small Reynolds number as estimated in Table 1 ($\mathbf{Re_g} = \boldsymbol{\rho_g u_d D_d/\mu_g}$, $\boldsymbol{\rho_g}$ and $\boldsymbol{\mu_g}$ are gas phase density and viscosity).

Table 1. Test cases parameters

	P_g (bar)	T_g (K)	T_d (K)	D_d (µm)	u_d (m/s)	Y_{C12H26}	Re_g
Case 1	62	700	363	38	0.0	0.999999	0
Case 2	88	1000	363	60	0.2	0.999999	9
Case 3	102	1200	363	60	0.2	0.999999	9
Case 4	102	1200	363	60	2	0.999999	86

3. Results and discussions

The results are organized as follows. Section 3.1 provides the qualitative verification for the proposed model in which the subcritical evaporation behaviors of isolated droplets are discussed. The phase state is observed based on the Tangent Plane Distance (TPD) information. Then in Section 3.2, a thoroughly thermodynamic analysis is carried out to better understand the transition from subcritical to supercritical regimes. Finally, conclusions will be presented in section 3.3.

3.1 VLE-diagram for n- dodecane/nitrogen mixture

A thorough equilibrium thermodynamic analysis for the n-dodecane/nitrogen phase change is performed in this Section. Figure 2 displays different thermodynamics' information. First, assuming the mixing between fuel and ambient gas to occur adiabatically, the mixture enthalpy (H_{AM}) at constant pressure can be expressed as [3],

$$H(T_{AM}, P) = z_{N2}\, H_{N2}(T_{N2}, P) + (1 - z_{N2})\, H_f(T_f, P) \quad (6)$$

where *H* and z_{N2} are the specific molar enthalpy and nitrogen mole fraction. Here, (T_{AM}) is the adiabatic mixing temperature (also denoted AMT), which is the unknown of Eq. (6). It is computed using a HP flash [36]. In single-phase state, the obtained T_{AM} is termed as "frozen temperature", (T_F, see the green curve in Figure 2). On the other hand, in two-phase states, the obtained T_{AM} is termed as, (T_E, see the red curve in Figure 2) when phase change is considered. Generally, the "frozen temperature", T_F, is lower than the equilibrium one T_E considering phase change. This is due to the well-known latent heat of vaporisation. As the ambient temperature increases, the difference between T_F and T_E decreases like the latent heat of vaporisation. Indeed, at 700 K (Case 1), the maximum difference between T_F and T_E is as large as 60 K in the region where z_{N2} is in the range (0.5 – 0.93), as shown in the images in Figure 2(a). On the contrary, as the ambient temperature is increased to 1200 K (Case 3), the gap between T_F and T_E decreases to less than 20 K.

In this work, all the scattered (blue) points depicted in Figure 2 are the numerical simulation results (Cases 1 and 3), which are obtained using the above tabulation method coupled to the HEM model (Eqs. (1)-(4)). The above numerical results accuracy in terms of T_E, as shown in Figure 2 demonstrate the correctness of the model [20]. Indeed, the scattered (blue) points are very close to the equilibrium temperature T_E curve, even though the internal energy rather than the total energy is transported in Eq. (4). It means that for the present simulations, the HEM model with internal energy is accurate enough to predict the mixing temperature evolution for evaporating droplets under Diesel conditions.

Figure2 also displays the T-x VLE diagram for n-dodecane/nitrogen mixture at 62 bar and 102 bar (Case 1 and 3) that was obtained from TP-flash [36]. The right (orange) dew line is the liquid phase equilibrium curve; the left (blue) bubble line is the gas phase equilibrium curve. The merge point of the two VLE lines is the mixture critical point ($T_{c,mix}, z_{c,mix}$). It is important to note that the two intersections resulting from the VLE lines and the AMT lines define the gas–liquid interface. Indeed, the intersection with the VLE liquid phase line defines the inner boundary of the interface (close to the liquid droplet core); and the intersection with VLE gas phase defines the outer interface boundary (close to the ambient gas). The area between the two intersections shows the range of N_2 concentration inside the two-phase interface. On the left side of the interface region, only liquid is present. In Case 3 for instance (Figure2(b)), up to 10% N_2 is dissolved in the liquid phase. While on the right side of the interface region, only gas is present and n-dodecane condensation cannot happen with a concentration less than about 15%.

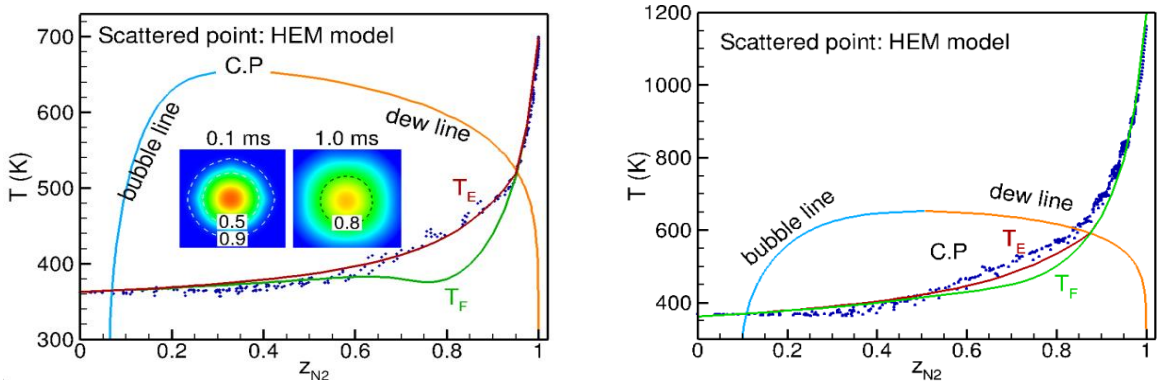

(a) Case 1: $T_g = 700$ K, $P_g = 62$ bar (b) Case 3: $T_g = 1200$ K, $P_g = 102$ bar

Figure 2. Temperature-composition phase diagram for $N_2 - C_{12}H_{26}$ mixture with frozen (T_F) and equilibrium (T_E) mixing temperature. Scattered data depicts the thermodynamic states obtained from the HEM model with tabulation approach.

3.2 Subcritical evaporation behaviours

Figure 3 depicts the time evolution of droplet evaporation behaviours under three conditions (Case 1 – 3, see Table 1). The numerical results in terms of density distribution at 0.1ms and 1ms are compared with the images (diffused back illumination) from Crua et al. [7]. The density distribution is displayed in the centre cut-plane of the droplets. In Case 1, the initial n-dodecane droplet diameter is set as 38μm based on the experimental observation [7]. Although, the droplet surface tension may have significant effects on the droplet deformation in such cool condition (700K), it has not been considered yet in our present model. This is the reason why the velocity is assumed negligible in this case to avoid non-physical droplet deformation. As the gas phase temperature becomes higher than 1000K (Cases 2 and 3), the droplet temperature at the outer interface boundary (as defined above in Figure 2(b)) rapidly increases close to $T_{c,mix}$ where surface tension almost vanishes. Therefore, the droplets velocity effects have been investigated under such high temperature by ignoring surface tension for Case 2 and 3. As a result, the n-dodecane droplet moving velocity is set as 0.2 m/s in Cases 2 and 3 in consistence with the experimental measurement [7].

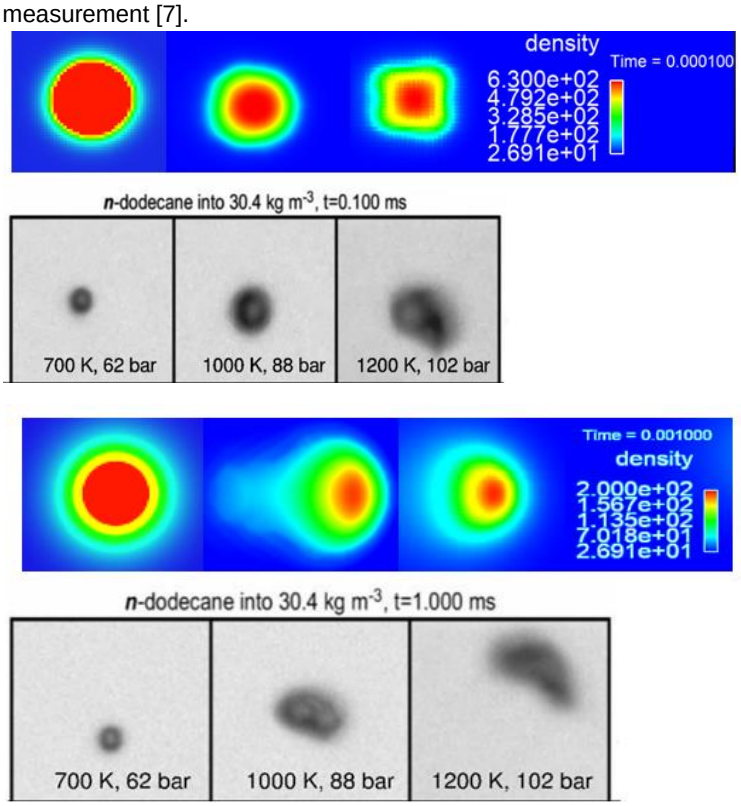

Figure 3. The evaporation behaviour of n-dodecane droplet under different ambient conditions. Comparison of the density distribution with the images from Crua et al. [7] (a) time = 0.1ms. (b) time = 1ms.

Because of the results presented in Figure 3, it was possible to obtain a good qualitative agreement between the experimental data and the predictions of the current HEM model. After the introduction of the droplet into nitrogen conditions (t = 0.1ms), a n-dodecane vapor boundary layer is formed at the droplet surface, and apparent

expansion behaviours are visible. The evaporation proceeds continuously, and all three droplets remain almost spherical, as shown in Figure 3, except in the 1200K where the droplet starts its deformation as in the experiments. Better initialization of the droplet should be improved to avoid this problem. After 1 ms, different behaviours are obtained for three cases, as shown in Figure 3(b). Case 1 remains spherical. However, for the moving droplets (cases 2 and 3), since the droplet centre with high density possesses large momentum and moves faster than the adjacent vapor, the droplets deform to an olive shape at 1 ms, which are similar to the experimental observations.

The evaporation characteristics are further studied by plotting the temperature, density, and TPD phase stability index contours, respectively, as Figure 4 under 1200 K and 102 bar (Case 3). Initially, the droplet remains spherical and then deforms progressively to an olive shape at 1ms. The density distribution exhibits distinct features from temperature distribution, indicating that the Lewis number associated with thermal and mass diffusion rates are not equal one. Also, no circulating eddy is found in the wake of droplet due to the low droplet velocity. The phase state is identified by the Tangent Plane Distance (TPD) index [4]: TPD = 0, 1, 2 correspond to single phase gas, single phase liquid and two-phase state, respectively. At initial time, the ambient is in pure gas state with TPD = 0 and the droplet is in pure liquid state with TPD = 1. Then, a two-phase diffused interface appears, as depicted by the red colour (TPD = 2) at t = 0.1 ms. Indeed, as the evaporation evolves, the droplet periphery changes to two-phase state. However, the droplet core is still in single-phase liquid state at 0.1 ms. Then, after t = 0.5 ms, single-phase liquid (TPD = 1) disappears, and the maximum density decreases from 630 to 410 kg/m^3 because more than 10% N_2 has dissolved in the liquid phase, as has been discussed above with Figure 2(b). At time t = 1 ms, the density of the two-phase droplet core has decreased further to 150 kg/m^3 because of the evaporation of n-dodecane and the diffusion of nitrogen. These diffusion processes are clearly promoted in the droplet wake, especially at t = 1 ms, as the droplet deforms to an olive shape. Finally, the evaporation seems to proceed until completing the entire evaporation of the liquid from two-phase core.

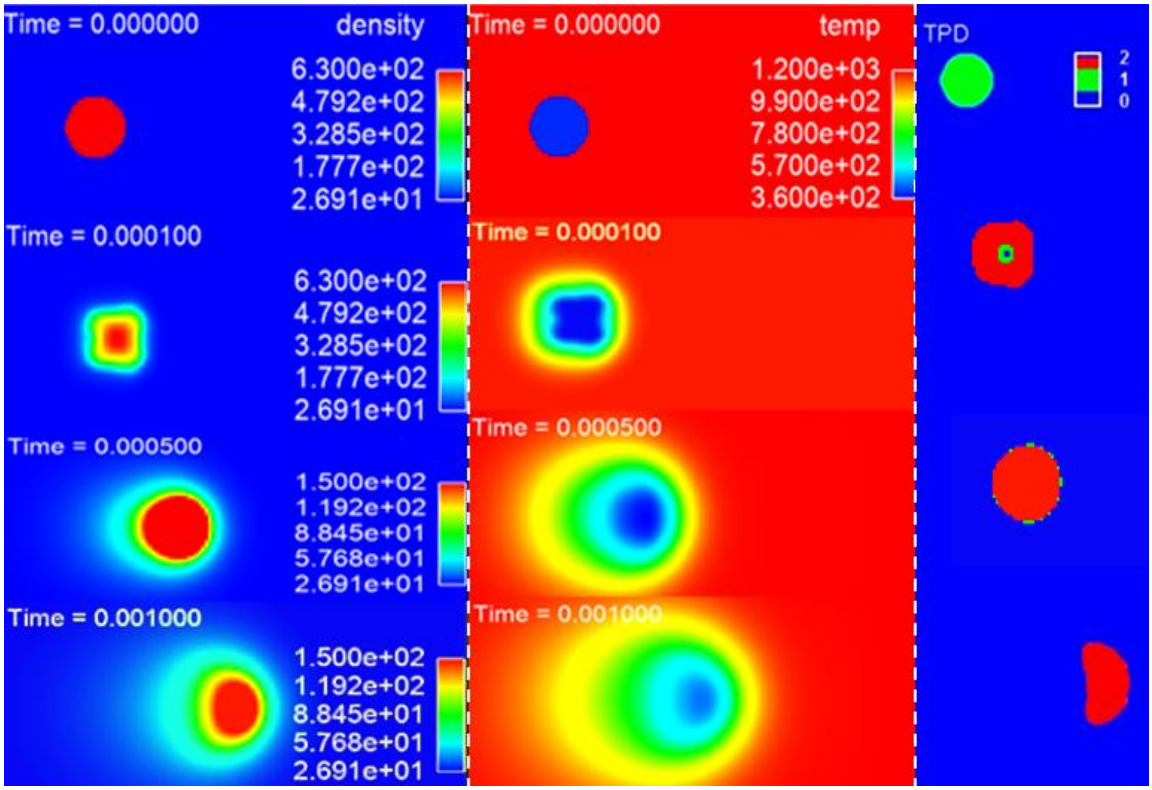

Figure 4. Distribution of density, temperature, and TPD (in the central cut-section) for the evaporating n-dodecane droplet with moving velocity of 0.2 m/s under 1200 K and 102 bar (Case 3). TPD=0 for gas; TPD=1 for liquid; TPD=2 for two-phase.

An additional test Case 4 has been simulated using a higher droplet initial velocities of 2m/s to investigate the effects of forced convection on the droplet dynamics and evaporation at the same condition as Case 3. In this study, various distinct phenomena can be highlighted from Figure 5. Primarily, the droplet deformation is substantially enhanced by the increased initial droplet momentum and the induced relative velocity between gas and liquid. The induced strong shear stress has led to a prompt breakup of liquid droplet. Also, As its obvious, the surface tension of the droplet comes to zero by growing the temperature of the droplet. Hence, the weber number of the droplet moves to infinity. As it has mentioned in the experimental study of Crua et al, We can observe that the droplet rapidly deforms, and it may experience an aerodynamic breakup process as bag breakup like.

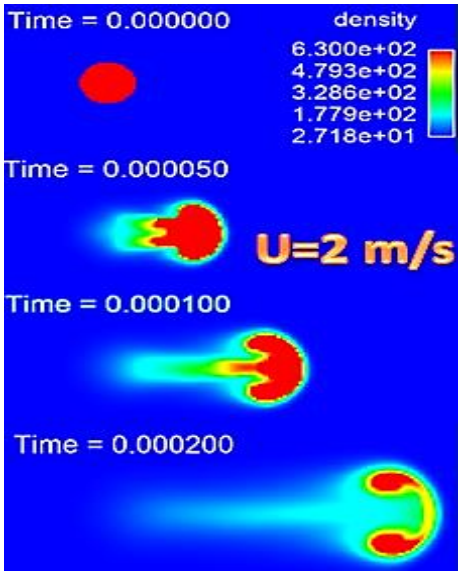

Figure 5. Density profile for the evaporation droplet of n-dodecane with moving velocity of **2m/s** under 1200 K and 102 bar.

Secondly, the droplet lifetime is much shorter than in by increasing the velocity. This is because the droplet breakup increases the interface area exposed to the hot ambient gas, thus it increases the evaporation rate. Thirdly, the evaporation rate is also enhanced by convective effects. Indeed, a thinner vapour layer near the droplet surface may be seen by increasing of the velocity.

3.3 Transcritical droplet behaviours

To get more insights into the thermodynamic behaviours of dodecane-nitrogen droplets three typical T-x diagrams are presented in Figure 6. They particularly focus on the phase state evolutions including the two-phase path, the single-tangent path, and the supercritical path. At the typical Spray A condition (60 bar and 900 K), the liquid droplet with the initial temperature of 363 K, is in single liquid-phase state for a while, and then it will transit to the two-phase state for most of its lifetime. In addition, as can followed up in the two-phase path in Figure 6(a), the droplet may evaporate completely if its temperature reaches a value higher than 550 K (temperature at the intersection of AMT curve with dew line). This is the first path to transit to the supercritical mixing state. The second path is when the droplet temperature T_d is greater than $670\ K$, (see Figure 6(a)). In this case, the droplet begins with single-liquid-like state. As the diffusion proceeds it goes through the mixture critical point (denoted as C.P) by tangent plane and then evolves to single-gas-like state. Here, we define this droplet temperature as a transcritical temperature $T_{trans\_droplet}$ for the corresponding condition ($60\ bar$ and $900\ K$). As the initial droplet temperature is larger than $T_{trans\_droplet}$, for instance $703\ K$ (see Figure 6(a)), the droplet transits from liquid-like to gas-like state directly without two-phase zone. As the ambient temperature and pressure increase, for instance to $1400\ K$ and $140\ bar$, the transcritical temperature $T_{trans\_droplet}$ reduces, as shown in Figure 6(b). Noteworthy, $T_{trans\_droplet}$ is very close to $T_{c,mix}$. As the maximum temperature and pressure in the large diesel engines are close or even larger than 2000K and 250bar, the transcritical temperature $T_{trans\_droplet}$ may reduce to lower than 500K, following $T_{c,mix}$. In such conditions, the spray is easy to transit to gas-like state, which may decrease liquid jet penetration significantly.

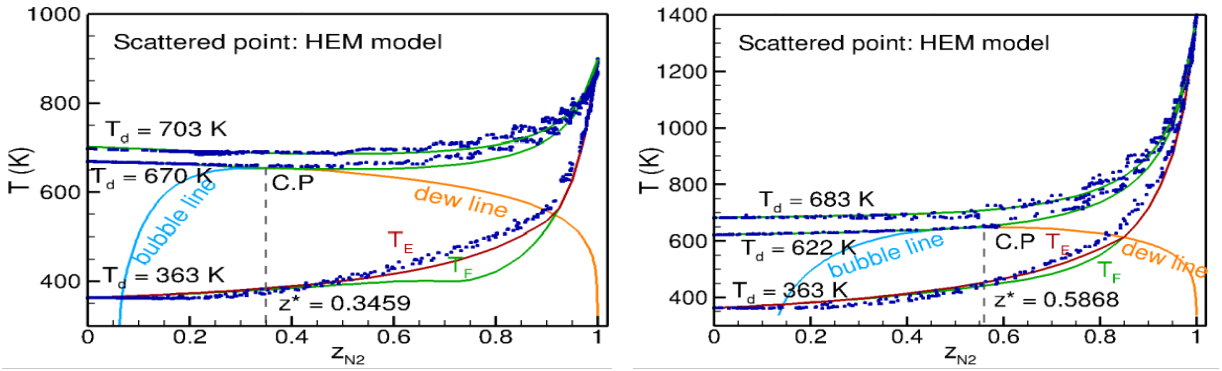

a) $T_g = 900$ K, $P_g = 60$ bar b) $T_g = 1400$ K, $P_g = 140$ bar

Figure 6. Temperature-composition diagram for N_2 – $C_{12}H_{26}$ mixture with frozen (T_F) and equilibrium (T_E) mixing temperature. Scattered data depicts the obtained data from the HEM model with tabulation approach.

3.4 Conclusions

A fully compressible multicomponent homogeneous equilibrium model (HEM) with a real-fluid equilibrium solver is developed. The phase change quantity as well as real-fluid thermal and transport properties are computed efficiently with a bijective tabulation method. The model predictions are validated qualitatively with the experimental observations. According to the numerical results, significant findings are obtained.

1. Classical evaporation is an important feature of a droplet in low and mild ambient temperature conditions. The droplet continuously evaporates with spherical shape.
2. As the ambient temperature and pressure increases above 1200K and 60bar, the moving droplet demonstrates significant deformations with the evaporation progressing, and deforms to olive shape, or even be shattered into fragments. This pertains to the droplet moving velocity, however it is still in the two-phase state based on the phase stability TPD method. In this condition, it can be concluded that the droplet is still in the subcritical evaporation regime.
3. The criterion for transition from liquid-like to gas-like state directly without two-phase state is provided and determined based on the ambient conditions as well as the initial (or possible transient) liquid temperature under diverse ambient conditions. These conditions will further be discussed in future works.

Acknowledgement

This project has received funding from the European Union Horizon 2020 Research and Innovation programme. Project IPPAD: Grant Agreement No 675528.

Reference

[1] Zhu G, Aggarwal S., 2000, International Journal of Heat and Mass Transfer, 43: 1157-1171.
[2] Bellan J., 2000, Progress in energy and combustion science, 26: 329-366.
[3] Qiu L, Reitz RD., 2015, International Journal of Multiphase Flow, 72: 24-38.
[4] Yang S, Habchi C, Yi P, Lugo R., 2018, ICLASS 2018, Chicago, USA.
[5] Polanco G., Holdo A. Munday G., 2010, Journal of Hazardous materials, 173(1-3):2-18
[6] Yang V., 2000, Proceedings of the Combustion Institute, 28: 925-942.
[7] Crua C, Manin J, Pickett LM., 2017, Fuel, 208: 535-548
[8] Dahms, Rainer N. Gradient, 2014, Journal of Colloid and Interface Science, 445C:48-59.
[9] Guiyuan Mo, Li Qiao.,2017, Combustion and Flame, 176. 60–71
[10] Hsieh K, Shuen J, Yang V., 1991, Combustion Science and Technology, 76: 111-132.
[11] Curtis E, Farrell P, 1992, Combustion and Flame, 90.
[12] Jia H, Gogos G., 1992, Journal of thermophysics and heat transfer, 6: 738-745.
[13] Baer M, Nunziato J., 1986, International journal of multiphase flow, 12: 861-889.
[14] Saurel R, Abgrall R., 1999, Journal of Computational Physics, 150: 425-467.
[15] Habchi C. 2015, Atomization and Sprays, 25(4):317-334.
[16] Kapila A, Menikoff R, Bdzil J, Son S, Stewart DS., 2001, Physics of fluids, 13: 3002-3024.
[17] Chiapolino A, Boivin P, Saurel R., 2017, Computers & Fluids, 150: 31-45.
[18] Saurel R, Boivin P, Le Métayer O., 2016, Computers & Fluids, 128: 53-64.
[20] Yi P, Yang S, Habchi C, Lugo R. 2019, Physics of Fluids, vol. 31, no. 2, p. 026102, 2019.
[21] Michelsen ML., 1999, State function-based flash specifications. Fluid Phase Equilibria, 158: 617-626.
[22] Saha S, Carroll JJ., 1997, The isoenergetic-isochoric flash. Fluid phase equilibria, 138: 23-41.
[23] Azimian AR, Arriagada JJ, Assadi M., 2004, Heat transfer engineering, 25: 41-51.
[24] Wang X-D, An B, Duan Y-Y, Wang Z-X et al.,2012, Journal of the Taiwan Institute of Chemical Engineers; 43.
[25] Wang X-D, Wang Z-X, Duan Y-Y, An B et al.,2014, Journal of the Taiwan Institute of Chemical Engineers, 45.
[26] Khatami F, Van Der Weide E, Hoeijmakers H., 2015, Heat transfer engineering, 36: 1065-1083.
[27] Brown S, Peristeras L, Martynov S, Porter R, Mahgerefteh H, Nikolaidis IK, Boulougouris GC, Tsangaris DM, Economou IG., 2016, Computers & Chemical Engineering, 95: 49-57.
[28] Chung TH, Ajlan M, Lee LL, Starling KE., 1988, Generalized multiparameter correlation for nonpolar and polar fluid transport properties. Industrial & engineering chemistry research, 27: 671-679.
[29] C. Ware, W. Knight, and D. Wells, 1991, Memory intensive algorithms for multibeam bathymetric data: Computers & Geosciences, 17, 985-993.
[30] Bohbot J, Gillet N, Benkenida A., 2009, IFP-C3D: an unstructured parallel solver for reactive compressible gas flow with spray. Oil & Gas Science and Technology-Revue de l'IFP, 64: 309-335.
[31] Michelsen ML., 1982, The isothermal flash problem. Part I. Stability. Fluid phase equilibria, 9: 1-19.
[32] Miller R, Harstad K, Bellan J., 1998, Evaluation of equilibrium and non-equilibrium evaporation models for many-droplet gas-liquid flow simulations. International Journal of Multiphase Flow, 24: 1025-1055.
[33] Ebrahimian V, Habchi C., 2011, Towards a predictive evaporation model for multi-component hydrocarbon droplets at all pressure conditions. International Journal of Heat and Mass Transfer, 54: 3552-3565.
[34] Yi P, Long W, Jia M, Tian J, Li B., 2016, Development of a quasi-dimensional vaporization model for multi-component fuels focusing on forced convection and high temperature conditions. International Journal of Heat and Mass Transfer, 97: 130-145.
[35] K. Saha, S. Som, & M. Battistoni, 2017, Investigation of homogeneous relaxation model parameters and their implications for gasoline injectors, Atomization and Sprays, (27), 4.
[36] Michelsen, M. L. (1985) Saturation point calculations. Fluid Phase Equilibria, 23(2-3), 181-192.
[37] Di Zhu, Ryosuke Okuno, 2016, Multiphase isenthalpic flash integrated with stability analysis, Volume 423, 15, Pages 203-219, https://doi.org/10.1016/j.fluid.2016.04.005